Pramana – J. Phys. (2018) 90:10
https://doi.org/10.1007/s12043-017-1499-4

© Indian Academy of Sciences

CrossMark

Minority heating scenarios in ^{4}He(H) and ^{3}He(H) SST-1 plasmas

ASIM KUMAR CHATTOPADHYAY

Institute for Plasma Research, Bhat, Gandhinagar 382 428, India
E-mail: asim@ipr.res.in

MS received 14 December 2016; revised 24 July 2017; accepted 1 August 2017;
published online 19 December 2017

Abstract. A numerical analysis of ion cyclotron resonance heating scenarios in two species of low ion temperature plasma has been done to elucidate the physics and possibility to achieve H-mode in tokamak plasma. The analysis is done in the steady-state superconducting tokamak, SST-1, using phase-I plasma parameters which is basically L-mode plasma parameters having low ion temperature and magnetic field with the help of the ion cyclotron heating code TORIC combined with 'steady state Fokker–Planck quasilinear' (SSFPQL) solver. As a minority species hydrogen has been used in ^{3}He and ^{4}He plasmas to make two species ^{3}He(H) and ^{4}He(H) plasmas to study the ion cyclotron wave absorption scenarios. The minority heating is predominant in ^{3}He(H) and ^{4}He(H) plasmas as minority resonance layers are not shielded by ion–ion resonance and cut-off layers in both cases, and it is better in ^{4}He(H) plasma due to the smooth penetration of wave through plasma–vacuum surface. In minority concentration up to 15%, it has been observed that minority ion heating is the principal heating mechanism compared to electron heating and heating due to mode conversion phenomena. Numerical analysis with the help of SSFPQL solver shows that the tail of the distribution function of the minority ion is more energetic than that of the majority ion and therefore, more anisotropic. Due to good coupling of the wave and predominance of the minority heating regime, producing energetic ions in the tail region of the distribution function, the ^{4}He(H) and ^{3}He(H) plasmas could be studied in-depth to achieve H-mode in two species of low-temperature plasma.

Keywords. Minority heating of ^{4}He(H) and ^{3}He(H) plasmas at low temperature; SST-1 tokamak; mode conversion.

PACS Nos 52.50.Qt; 52.55.Fa

1. Introduction

Ion cyclotron resonance frequency (ICRF) wave heating is an attractive option to achieve an H-mode in tokamak plasma. For low-temperature plasma there are two options – second harmonic heating of the single species plasma or minority heating at the fundamental in a two-species plasma. It is known that the former is quite inefficient particularly for low-temperature plasma. Hence, it is important to study the fundamental physics associated with minority heating by ICRF wave in order to assess its feasibility for achieving H-mode. To the best of the author's knowledge, the wave absorption scenarios in two-species low-temperature plasma have not been studied properly so far. This work is one such attempt where a numerical analysis of ion cyclotron resonance heating (ICRH) scenarios in two-species plasma has been studied using plasma parameters of phase I operation of SST-1 tokamak [1] which are essentially L-mode plasma parameters having low ion and electron temperature (see table 1).

Minority heating is studied after taking hydrogen (H) as the minority species in ^{3}He/^{4}He plasma. The helium plasma with minority heating is also very crucial for ITER to achieve H-mode during non-activated operation phase. The numerical analysis is done with the help of ion cyclotron resonance heating code TORIC [2] coupled with SSFPQL module [3].

The TORIC is a finite Larmour radius (FLR) full wave code which solves the wave equation in general toroidal axisymmetric configurations. The wave equation is derived from Vlasov equation by expanding the electromagnetic fields in Fourier modes in toroidal and poloidal angles. The code TORIC describes the propagation and absorption at fundamental ($\omega = \Omega_{ci}$) and second harmonic ($\omega = 2\Omega_{ci}$) ion cyclotron resonance frequencies, whereas electron absorption is via electron Landau damping (ELD), transit time magnetic pumping

Table 1. Plasma and other parameters chosen for simulation of ion cyclotron resonance heating scenarios of SST-1 in phase-I operation.

Major radius	110 cm
Minor radius	20 cm
Magnetic field	1.5 Tesla
Toroidal current	100 kA
Central electron density	2.0×10^{13} cm^{-3}
Central electron temperature	0.500 keV
Central ion temperature	0.200 keV
Electron density at separatrix	2.0×10^{12} cm^{-3}
Electron and ion temperature at separatrix	0.02 keV
Applied wave frequency	22.8 MHz
Representative toroidal wave number	16

(TTMP), and the cross-term absorption. TORIC can also model ion Bernstein wave (IBW) and ion cyclotron wave (ICW) at the ion–ion resonance layer [2]. A detailed description is given in ref. [2].

SSFPQL solves the steady-state surface-averaged quasilinear Fokker–Planck equation for ions heated at the fundamental and second harmonic cyclotron frequencies and evaluate the distribution function, using the quasilinear diffusion coefficients for each magnetic surface evaluated by TORIC. The output of the full-wave TORIC code, viz. magnetic surface-averaged power deposition profile, is exported to SSFPQL. Once the quasilinear distribution function of the ions has been evaluated by SSFPQL, the module QLMINH makes TORIC to estimate the influence of the suprathermal population on wave propagation and absorption [3]. So, TORIC and SSFPQL are interlinked. SSFPQL provides information also on the radial profiles of parallel and perpendicular energies, number of fast ions of high-energy (suprathermal) tail generated by ion cyclotron resonance heating, information on the collisional exchanges between these tails and background ions and electrons etc. besides the distribution functions.

The rest of the paper is arranged as follows: Section 2 describes a brief theory of ICRF waves in two-species plasma, minority heating model, and mathematical description used in TORIC-SSFPQL module. Section 3 is dedicated for results and discussion, whereas §4 summarises the results.

2. Theory and numerical model

2.1 *A brief theory of ICRF wave in two-species plasma*

In plasma with several ion species having different charge to mass ratios, there is an additional resonance and associated cut-off between each pair of ion cyclotron frequencies. The additional resonance layer is called ion–ion hybrid, or *Buchsbaum*, resonance and the cut-off layer is called the ion–ion cut-off layer. These layers play important roles in minority heating which will be discussed in the next subsection.

Simple cold plasma dispersion relation (eq. (1)) for fast wave can be used to get the positions of ion–ion resonance and cut-off with sufficient accuracy [4].

$$n_\perp^2 = \frac{\left(L - n_{||}^2\right)\left(R - n_{||}^2\right)}{\left(S - n_{||}^2\right)}. \tag{1}$$

Here $n_\perp$ and $n_{||}$ are respectively the plasma refractive indices perpendicular and parallel to the static magnetic field, whereas L, R, S are the dielectric tensor elements in Stix notation [5]. For waves in ICRF range, it can be shown [4] that

$$\begin{aligned} R &\simeq \sum_i \frac{\omega_{pi}^2}{\Omega_{ci}(\Omega_{ci} + \omega)}, \\ L &\simeq \sum_i \frac{\omega_{pi}^2}{\Omega_{ci}(\Omega_{ci} - \omega)}, \\ S &\simeq \sum_i \frac{\omega_{pi}^2}{(\Omega_{ci}^2 - \omega^2)}. \end{aligned} \tag{2}$$

Sum is over all the ion species, i. ω_{pi} is the ion plasma frequency, Ω_{ci} is the ion cyclotron resonance frequency at the point concerned, and ω is the applied frequency. Cut-off occurs when $L = n_{||}^2$ or $R = n_{||}^2$; resonance occurs when $S = n_{||}^2$. For two-ion species in a quasineutral plasma the ion–ion resonance and cut-off conditions are

$$\begin{aligned} &S = n_{||}^2, \quad \text{for ion}-\text{ion resonance} \\ &L = n_{||}^2, \quad \text{for ion}-\text{ion cut-off}. \end{aligned} \tag{3}$$

Furthermore, L and S are of the order $\sum_i(\omega_{pi}^2/\Omega_{ci}^2) = O(m_i/m_e)$, times a factor depending on ω/Ω_{ci} which is itself numerically large [4]. Therefore, taking realistic values of $n_{||}^2$ we can write eq. (3) without appreciable error

$$\begin{aligned} &S = 0, \quad \text{for ion}-\text{ion resonance} \\ &L = 0. \quad \text{for ion}-\text{ion cut-off}. \end{aligned} \tag{4}$$

To solve eq. (4), we introduce the number concentration of species i

$$\nu_i = n_i/n_e, \quad \sum_i Z_i \nu_i = 1$$

and take the relation [4] $\omega_{pi}^2/\Omega_{ci}^2 \propto \nu_i A_i$, $\omega/\Omega_{ci} \propto A_i/Z_i$ to eliminate plasma frequency. Here $Z_i\nu_i$ is the

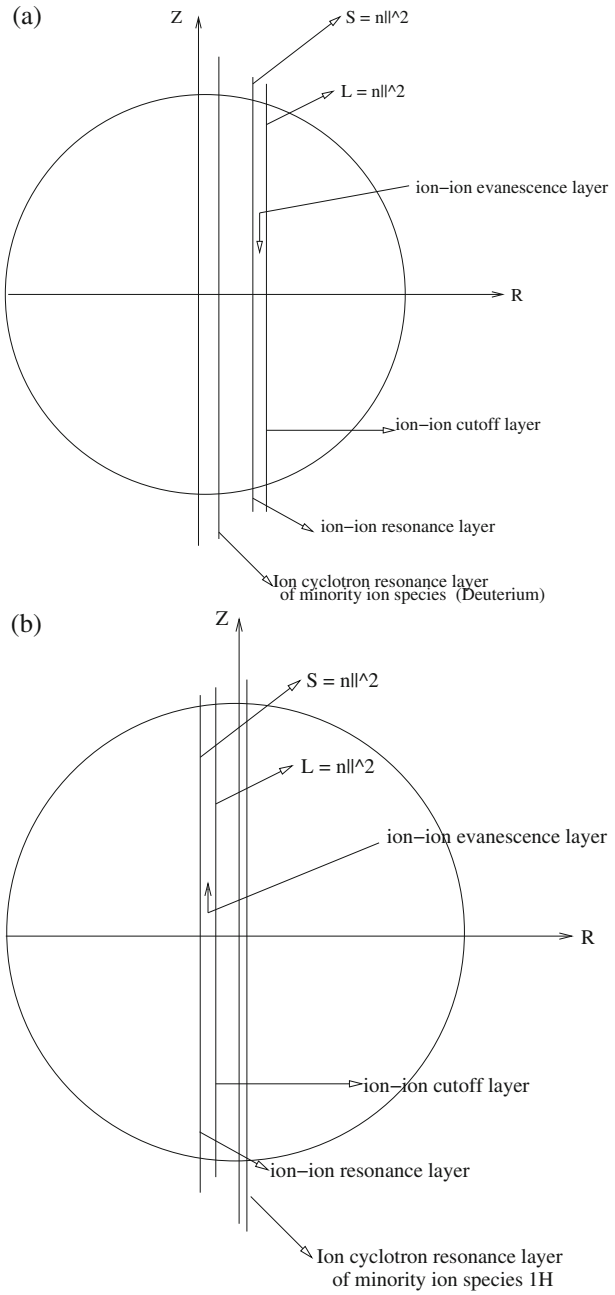

Figure 1. A sketch showing the position of ion–ion cut-off, ion–ion resonance, and ion cyclotron resonance layer (fundamental) of the minority species for (**a**) H(D) plasma and (**b**) ^{3}He(H)/^{4}He(H) plasma. Positions of different layers are enlarged to show them clearly (for details, see text).

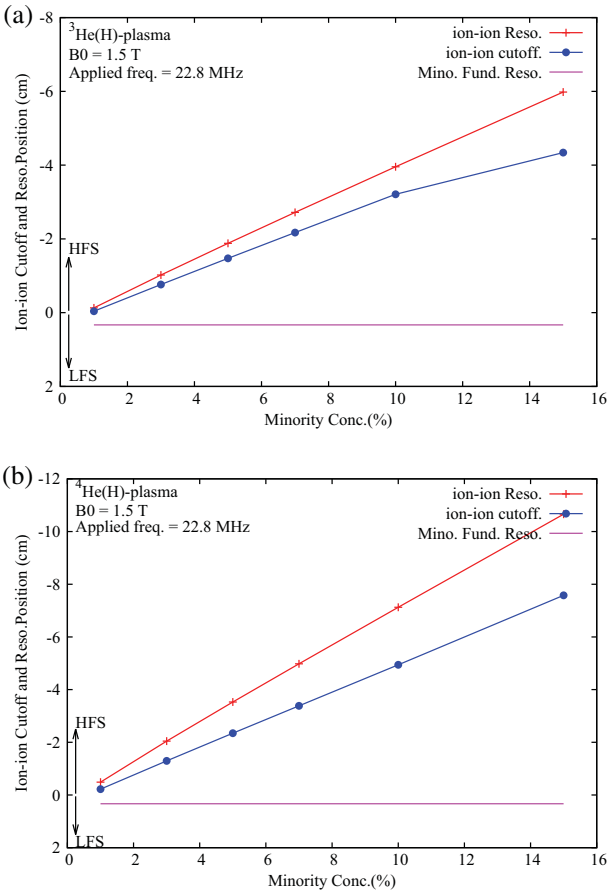

Figure 2. The position of ion–ion resonance, cut-off and minority resonance layers with minority concentration in (**a**) ^{3}He(H) plasma and (**b**) ^{4}He(H) plasma for minority heating. In both cases, minority resonance layers are not shielded by ion–ion cut-off and resonance layers. In the figures, zero is the poloidal centre of the tokamak. The abbreviation 'HFS' and 'LFS' indicate the high field side and low field side of the tokamak. The rf wave is launched from the low field side.

fraction of electrons contributed by species, i. In the above equations, n_i and n_e are the density of ion species, i, and that of electrons respectively, whereas Z and A indicate the atomic and mass numbers of the ion species.

Denoting the minority species with the index m and majority with M the solution of eq. (4) can be written in terms of the concentration and the ratio ω/Ω_c of minority species as [4]

$$\left.\frac{\omega^2}{\Omega_{\rm cm}^2}\right|_{\rm res} = \frac{1+\nu_m Z_m\left(\frac{Z_M/A_M}{Z_m/A_m}-1\right)}{1+\nu_m Z_m\left(\frac{Z_m/A_m}{Z_M/A_M}-1\right)} \tag{5}$$

and

$$\left.\frac{\omega}{\Omega_{\rm cm}}\right|_{\rm cof} = 1+\nu_m Z_m\left(\frac{Z_M/A_M}{Z_m/A_m}-1\right). \tag{6}$$

The subscripts 'res' and 'cof' indicate resonance and cut-off respectively. Finally, eqs (5) and (6) written in terms of $\omega/\Omega_{\rm cm}$ can be written into equations specifying the positions of ion–ion resonance and cut-off in a tokamak using the relation

$$\Omega_{\rm cm}(X) = \Omega_{\rm cm}(R_0)\frac{R_0}{(R_0+X)}, \tag{7}$$

Table 2. Fundamental and second harmonic resonance layers of the ion species in ^{3}He(H) and ^{4}He(H) plasmas. Table also shows the position of ion–ion cut-off and resonance layers inside the plasma. Applied frequency for minority heating of both ^{3}He(H) and ^{4}He(H) plasmas is 22.8 MHz at $B_0 = 1.5$ Tesla. Negative sign before the data indicates that the position of the corresponding layer is left of the poloidal centre and at high field side.

Plasma	Minority concentration (%)	Fundamental resolution (cm)	2nd harmonic resolution (cm)	Ion–ion resonance (cm)	Ion–ion-cut off (cm)
		^{3}He H	^{3}He H		
^{3}He(H)	0.5	OP* 0.332	OP OP	–	–
	1	OP 0.332	OP OP	−0.129	−0.039
	3	OP 0.332	OP OP	−1.020	−0.763
	5	OP 0.332	OP OP	−1.880	−1.472
	7	OP 0.332	OP OP	−2.719	−2.171
	10	OP 0.332	OP OP	−3.955	−3.210
	15	OP 0.332	OP OP	−5.981	−4.339
		^{4}He H	^{4}He H		
^{4}He(H)	0.5	OP 0.332	0.332 OP	−0.084	0.053
	1	OP 0.332	0.332 OP	−0.489	−0.222
	3	OP 0.332	0.332 OP	−2.044	−1.296
	5	OP 0.332	0.332 OP	−3.530	−2.345
	7	OP 0.332	0.332 OP	−4.980	−3.383
	10	OP 0.332	0.332 OP	−7.124	−4.940
	15	OP 0.332	0.332 OP	−10.659	−7.578

*OP ⇒ Outside the plasma.

where X is the horizontal distance from the magnetic axis and R_0 is the radius of the torus. Equations (5), (6) and (7) can be used explicitly to find out the positions of ion–ion resonance and ion–ion cut-off with minority concentration.

2.2 *Minority heating model*

The wave electric field of FW is elliptically polarised and therefore, we can divide the electric field component perpendicular to the background magnetic field in two components: one component (E_+) rotates in the same direction as the ions and the other component (E_-) in counter rotation. To the lowest order, it is the E_+ component that gives rise to absorption.

The fundamental ICRF wave heating of the single species plasma is usually weakly efficient due to unfavourable fast wave (FW) polarisation at $\omega = \Omega_{ci}$ [4,6]. The low efficiency is due to the screening of E_+ component of the electric field of radio frequency (RF) wave which is responsible for ion heating. To avoid this screening, one usually uses plasma containing two-ion species with different charge to mass ratio [7].

Depending on minority/majority density ratio, two heating regimes may be identified. The first regime is the minority heating (MH) where small minority concentration is used. This regime is characterised by the generation of suprathermal minority ions, which indirectly leads to bulk ion and electron heating. The second regime which is obtained by increasing minority concentration is called mode-conversion (MC) regime. In this regime, the FW is partially converted to short wavelength mode at the ion–ion hybrid resonance layer. The converted wave is commonly absorbed by electrons in the narrow region. In contrast to the indirect bulk plasma heating observed in MH scenario, the MC regime is characterised by a direct localised electron heating that occurs on a short time scale of the electron–electron collision.

Figure 1 shows a sketch of the positions of ion–ion resonance, ion–ion cut-off, mode conversion, and evanescence layers for H(D) and ^{3}He(H)/^{4}He(H) plasmas. In H(D) plasma (figure 1a) ion cyclotron resonance layer of the minority species (D) is shielded by the mode-conversion layer near ion–ion resonance layer in low field side, whereas in ^{3}He(H)/^{4}He(H) plasma ion cyclotron resonance layer of the minority species is not shielded by mode-conversion layer (figure 1b). From figure1a it is observed that both ion–ion resonance layer (IIRL) for $S = n_\parallel^2$ and cut-off layer (IICL) for $L = n_\parallel^2$ are within the plasma and on the low field side. Ion–ion evanescence layer (IIEL) is bounded by IIRL and IICL. It is to be noted that transition to MC region starts when $S = n_\parallel^2$ resonance emerges from the Doppler-broadened cyclotron resonance layer, which happen when minority concentration is larger than the critical value [4]. The position of MC layer of the H(D) plasma is in low field side

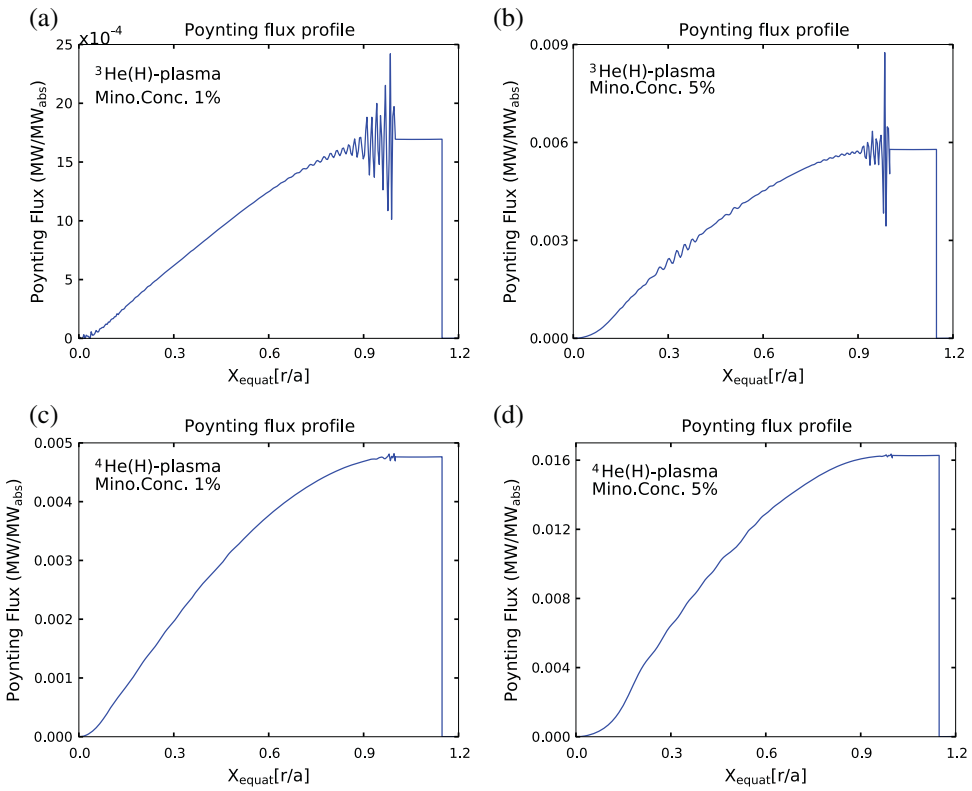

Figure 3. (**a**) and (**b**) are the Poynting flux profiles of ^{3}He(H) plasma due to minority heating at 1% and 5% minority concentration on the equatorial plane. Coupling of wave at plasma–vacuum interface is not so good. (**c**) and (**d**) are those of ^{4}He(H) plasma at the same minority concentration. Coupling of waves at plasma–vacuum interface is good. The antenna position (3 cm from the scrape-off edge of the plasma) is at the low field side and at 1.15 in terms of the normalised radial position on the equatorial plane, $X_{\text{equat}}[r/a]$. Normalisation is done with the minor radius of the tokamak. Unit of the Poynting flux indicates the value of the physical quantity for 1 MW coupled power.

compared to that of ion cyclotron resonance layer of the minority species (D). As a result, fundamental cyclotron resonance layer of the minority species is shielded by mode-conversion layer. So, ^{3}He(H) and ^{4}He(H) are good two-species plasmas for studying minority heating scenarios.

2.3 *Mathematical background of TORIC code and SSFPQL module*

TORIC solves the following inhomogeneous Maxwell's equations in the presence of plasma:

$$\vec{\nabla} \times (\vec{\nabla} \times \vec{E}) = \frac{\omega^2}{c^2}\left(\vec{E} + \frac{4\pi i}{\omega}\vec{J}^P\right), \tag{8}$$

where $\vec{J}^P$ is the high-frequency (hf) plasma current, $\vec{E}$ is the wave electric field, and ω is the applied angular frequency. Using linearised Vlasov equation and constitutive relation in FLR approximation, hf plasma current $\vec{J}^P$ can be expressed as a function of $\vec{E}$ [2,8] and takes the form:

$$\vec{J}^P = \vec{J}^0 + \sum_s \vec{J}_s^{(2)}. \tag{9}$$

Summation is over all species, s, and superscripts on the terms on right-hand side of eq. (9) indicate the order of expansion. $\vec{J}^0$ denotes the zero-order Larmour radius current and the second term on the right-hand side of eq. (9) is ions and electrons FLR currents. FLR expansion makes sense only when it can be stopped at second order which describes pressure-driven waves. It is extremely tedious to calculate FLR expansion beyond second order, and in most cases they do not describe any physical meanings [2]. All 'diamagnetic' contributions to the hf plasma current $\vec{J}^P$ (i.e. terms proportional to $\nabla n, \nabla T_i, \nabla T_e$ where n, T_i, T_e are the plasma density, ion, and electron temperatures respectively) have been neglected. Omitting these terms eliminates the drift branch of dispersion relation, but has a negligible influence on waves in the IC frequency range [2].

The numerical solution of the above wave equation is based on the spectral representation of the wave field $\vec{E}$ in poloidal angle θ and toroidal angle ϕ, and

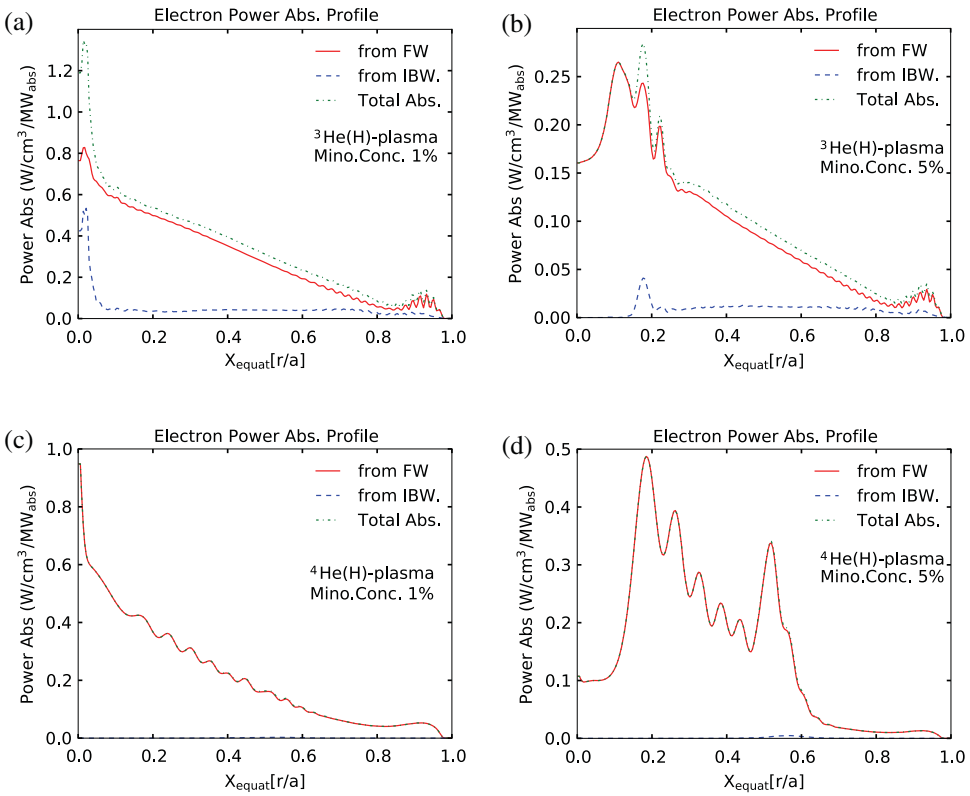

Figure 4. (**a**) and (**b**) are the electron power absorption profiles for different processes at minority concentration 1% and 5% respectively for ^{3}He(H) plasma, whereas (**c**) and (**d**) are the same results at the above minority concentration for ^{4}He(H) plasma due to minority heating on the equatorial plane. The power absorption by electron from IBW in ^{4}He(H) plasma is so small compared to that from FW that it lies on the horizontal axis (for details, see table 3). $X_{\text{equat}}[r/a]$ is the radial position normalised to plasma minor radius on the equatorial plane. Unit of power density indicates the absorption of power per unit volume for 1 MW coupled power.

a radial decomposition using cubic Hermite finite elements method as follows [2]:

$$\vec{E} = \sum_{m_\theta, n_\phi} \vec{E}^{m_\theta, n_\phi}(r) \mathrm{e}^{i(m_\theta \theta + n_\phi \phi)}, \tag{10}$$

where m_θ and n_ϕ are poloidal and toroidal mode numbers respectively. A weak formulation of the wave equation is used which is done with the help of standard Galarkin's method. Suitable regulatory conditions on the magnetic axis as well as boundary conditions at the plasma edge, Faraday shield, antenna, and wall are used to solve wave equation with the finite element method. A detailed description of these boundary conditions could be found in [2].

The module SSFPQL is based on the quasilinear kinetic equation:

$$\frac{\mathrm{d}F_i}{\mathrm{d}t} = \left(\frac{\partial F_i}{\partial t}\right)_{\text{QL}} + \left(\frac{\partial F_i}{\partial t}\right)_{\text{coll}} + \left(\frac{\partial F_i}{\partial t}\right)_{\text{loss}}. \tag{11}$$

The term $\mathrm{d}F_i/\mathrm{d}t$ on the left-hand side of eq. (11) is the evolution of distribution function with time, whereas the first term $(\partial F_i/\partial t)_{\text{QL}}$ on the right-hand side is the quasilinear operator, the second term $(\partial F_i/\partial t)_{\text{coll}}$ is the Fokker–Planck collisional operator, and the third term $(\partial F_i/\partial t)_{\text{loss}}$ is the loss term. It is to be noted that the quasilinear diffusion coefficient involved with $(\partial F_i/\partial t)_{\text{QL}}$ has a strong pitch angle, μ, dependence.

The SSFPQL solves the following steady-state $((\mathrm{d}F_i/\mathrm{d}t) = 0)$ quasilinear kinetic equation for IC heated ions [9], neglecting the loss term.

$$0 = \left(\frac{\partial F_i}{\partial t}\right)_{\text{QL}} + \left(\frac{\partial F_i}{\partial t}\right)_{\text{coll}} + S_i(v). \tag{12}$$

The isotropic source term, $S_i(v)$, is added to maintain different background species at different temperatures in the absence of hf wave heating. It is to be noted that SSFPQL is based on a rather simplified model. It takes surface-averaged, uniform-plasma Kennel–Engelmann quasilinear operator [9] neglecting the effect of toroidocity on IC heating, viz. toroidal trapping, finite banana width, and loss. It also takes that the collisional operator is linearised, assuming that the fast ion distribution function reaches steady state by losing energy on the background ions and electrons. For

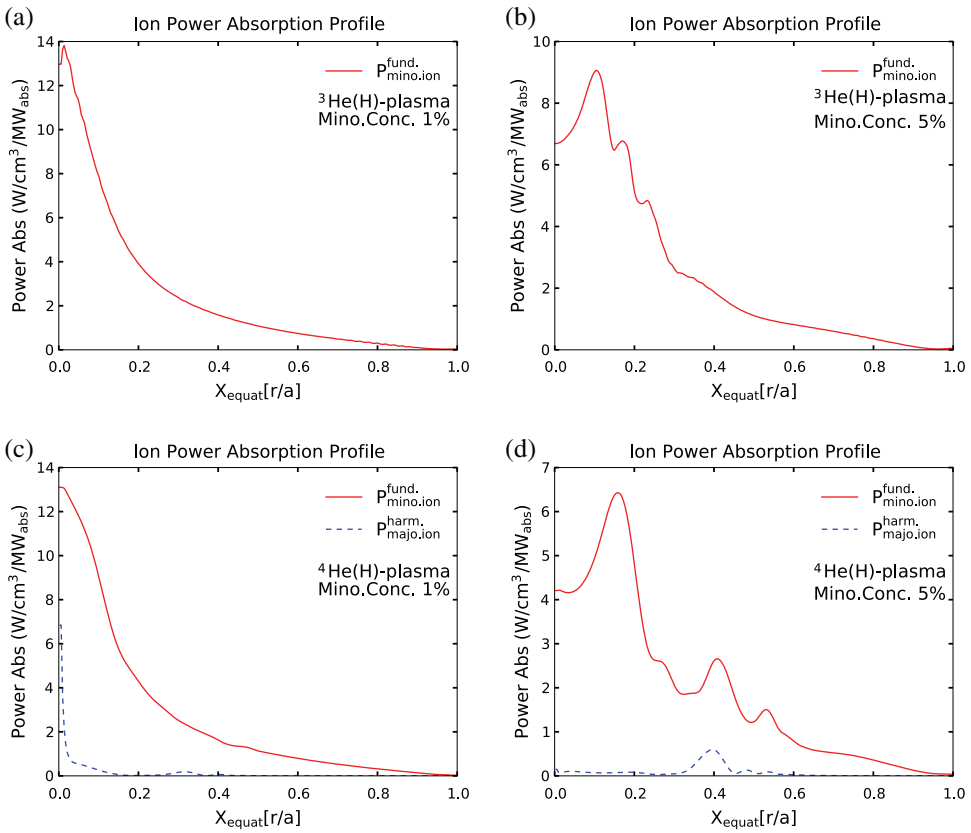

Figure 5. (**a**) and (**b**) are the ion power absorption profiles at minority concentration 1% and 5% respectively for ^{3}He(H) plasma, whereas (**c**) and (**d**) are the same results at the above minority concentration for ^{4}He(H) plasma due to minority heating on the equatorial plane. The radial position ($X_{\text{equat}}[r/a]$) is normalised to the minor radius. Unit of power density indicates the absorption of power per unit volume for 1 MW coupled power.

these assumptions, SSFPQL is not the full substitute of the sophisticated Fokker–Planck solver or Monte Carlo simulations, particularly for the most energetic ions.

3. Results and discussion

The plasma parameters chosen for the phase-I operation of SST-1 for these numerical works are tabulated in table 1. The applied wave frequency in both ^{3}He(H) and ^{4}He(H) plasmas is chosen as 22.8 MHz which is the fundamental cyclotron frequency of the minority ion H in 1.5 Tesla magnetic field ('minority heating'). The ^{4}He(H) plasma is like D(H) plasma and in both cases fundamental resonance frequency of the minority ion is equal to the second harmonic resonance frequency of the majority.

Figure 2 shows the ion–ion cut-off, resonance, and minority ion cyclotron resonance layers in ^{3}He(H) and ^{4}He(H) plasmas with minority concentration. Unlike H(D) plasma, minority ion cyclotron resonance layer is not shielded by ion–ion cut-off layer in ^{3}He(H) and ^{4}He(H) plasmas. Ion–ion cut-off and resonance layers shift gradually towards high field side with the increase of minority concentration, e.g. at minority concentration 1% the ion–ion resonance and ion–ion cut-off layers in ^{3}He(H) plasma are at 0.129 cm and 0.039 cm respectively from the poloidal centre towards high field side, whereas those positions at 15% minority concentration are at 5.981 cm and 4.339 cm respectively from the poloidal centre towards high field side; but this shift is more in ^{4}He(H) plasma which are 0.489 cm and 0.222 cm respectively from poloidal centre towards high field side at minority concentration 1% and 10.659 cm and 7.578 cm respectively from the poloidal centre towards high field side at concentration 15% respectively. Table 2 enumerates the positions of different plasma layers for minority heating of ^{3}He(H) and ^{4}He(H) plasmas for ready reference. The negative data in the table indicates that the position of the layer is towards the left of the poloidal centre and to the high field side. Both second harmonic resonance layers of ^{3}He and H ion species as well as fundamental resonance layer of ^{3}He ion species in ^{3}He(H) plasma lie outside the plasma (denoted by 'OP' in table), whereas fundamental resonance layer of ^{4}He and second harmonic resonance

layer of H ion species in ^{4}He(H) plasma lie outside the plasma for chosen plasma parameters, magnetic field, and wave frequency.

The coupling of rf wave at the plasma–vacuum interface and penetration of wave inside the plasma are judged with the help of Poynting flux profile in equatorial plane (figure 3) indicating the power transported by the fields across the surface [10]. $X_{\text{equat}}[r/a]$ in figures is the normalised minor radius on equatorial plane and the unit of flux implies Poynting flux per MW coupling of total power. It is observed that coupling is better in ^{4}He(H) plasma (figures 3c and 3d) than that in ^{3}He(H) plasma (figures 3a and 3b) due to minority heating with 1% and 5%. Smooth entry of the rf wave through plasma–vacuum surface depends on the plasma surface impedance, Z_p (ratio of E_y and B_z of the rf wave at plasma surface calculating from plasma side) which in turn depends mainly on plasma parameters at the edge region. Mismatching of impedances at plasma–vacuum surface calculating from both vacuum side (Z_v) and plasma side (Z_p) hinders smooth wave penetration. Smooth penetration of the wave under the chosen plasma parameters in ^{4}He(H) plasma shows good coupling and makes it a better two-species plasma to study rf wave absorption scenarios in SST-1 plasma parameters range.

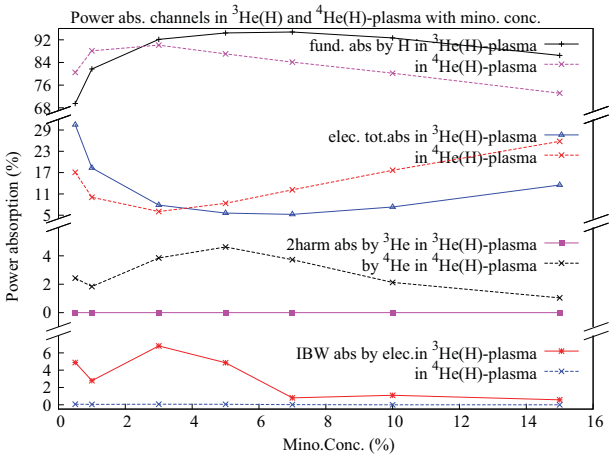

Figure 6. The figure shows different power absorption channels for minority heating in ^{3}He(H) and ^{4}He(H) plasmas with minority concentration. The top panel of the figure is the fundamental power absorption of minority species, 'H' in ^{3}He(H) and ^{4}He(H) plasmas. Second panel from the top is the electron total power absorption with minority concentration. Third panel from the top of the figure is the second harmonic power absorption by majority species in ^{3}He(H) and ^{4}He(H) plasmas, whereas bottom panel of the figure shows the electron power absorption from IBW with concentration of minority species. For details, see text.

Figures 4 and 5 show electron and ion power absorption profiles vs. normalised radius respectively in ^{3}He(H) and ^{4}He(H) plasmas with minority concentration 1% and 5% through different channels on equatorial plane. Power absorption by electron from IBW due to Landau damping is very small both in ^{3}He(H) and ^{4}He(H) plasmas compared to the power absorption from FW as shown in figure 4. IBW absorption by electron in ^{4}He(H) plasma is too small (4c, 4d) compared to that in ^{3}He(H) plasma (4a, 4b). More shifting of ion–ion resonance layers towards in-board in high field side in ^{4}He(H) plasma (table 2) compared to that in ^{3}He(H) plasma might be a reason for less production of IBW

Table 3. Power absorption through different channels in ^{3}He(H) and ^{4}He(H) plasmas. Applied frequency for minority heating is 22.8 MHz at $B_0 = 1.5$ Tesla.

Plasma	Minority concentration (%)	Fundamental ion absorption (%)		2nd harmonic ion absorption (%)		Total electron absorption (%)	IBW absorption (%)
		^{3}He	H	^{3}He	H		
^{3}He(H)	0.5	0	69.52	0	0	30.48	4.89
	1.0	0	81.69	0	0	18.31	2.78
	3.0	0	92.16	0	0	7.84	6.80
	5.0	0	94.41	0	0	5.59	4.89
	7.0	0	94.76	0	0	5.24	0.80
	10.0	0	92.68	0	0	7.32	1.10
	15.0	0	86.49	0	0	13.51	0.57
		^{4}He	H	^{4}He	H		
^{4}He(H)	0.5	0	80.48	2.43	0	17.09	0.07
	1.0	0	88.12	1.84	0	10.04	0.05
	3.0	0	90.13	3.85	0	6.03	0.07
	5.0	0	87.04	4.62	0	8.35	0.06
	7.0	0	84.12	3.73	0	12.14	0.02
	10.0	0	80.22	2.13	0	17.66	0
	15.0	0	73.14	1.04	0	25.82	0

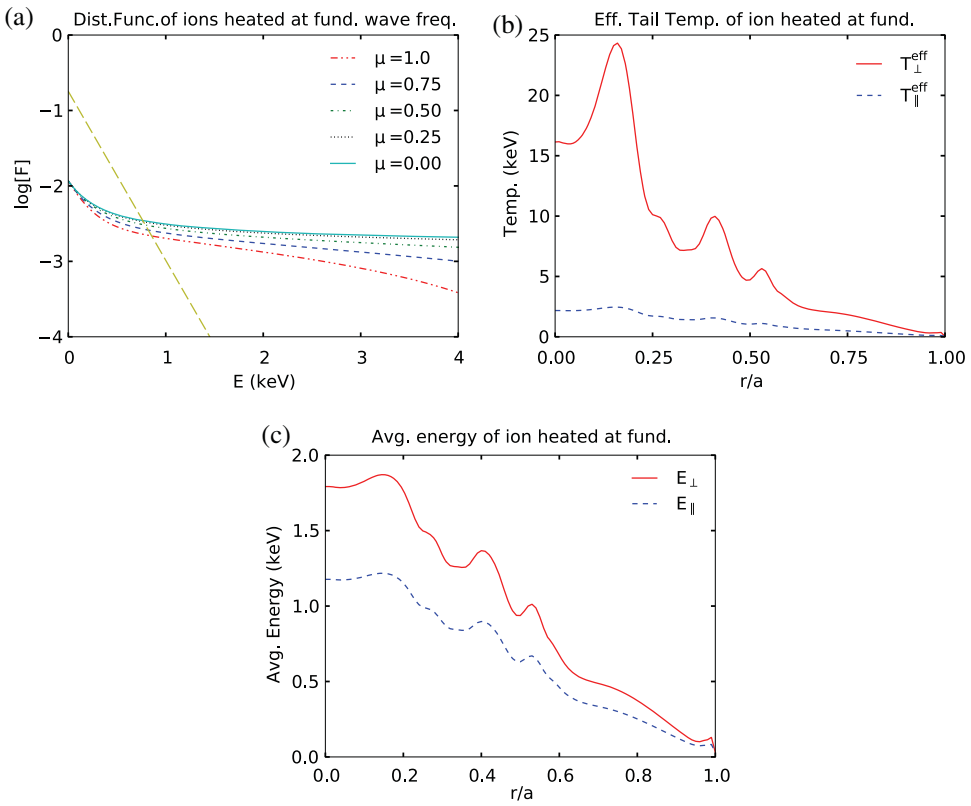

Figure 7. (**a**) Semi-log plots of quasilinear distribution function vs. energy at five values of the pitch angle (μ), at the position of peak absorption for the minority ion (hydrogen) heated at the fundamental. (**b**) shows the effective parallel and perpendicular tail temperature whereas (**c**) shows the effective average energy of the minority ion vs. normalised radius for a total coupled power of 0.1 MW. The long dashed curve is the unperturbed Maxwellian at the peak absorption position and a background temperature of 0.200 keV.

near ion–ion resonance layer in ^{4}He(H) plasma and hence less absorption of IBW by electron. Figures 5a and 5b show that in ^{3}He(H) plasma there is no second harmonic power absorption by ^{3}He ion as second harmonic resonance layer lies outside the plasma (table 2), whereas in ^{4}He(H) plasma second harmonic resonance layer lies inside the plasma and the power absorption by ^{4}He ion around this layer is less (figures 5c, 5d). This is due to the reason that second harmonic resonance heating is a finite Larmour radius effect which depends on ion temperature. With the increase of minority concentration power absorption profiles of electron and ion become broader and non-monotonic in both cases (figures 4 and 5). Non-monotonic nature is more prominent in electron absorption profile than in ion absorption profile. This may be due to low temperature of plasma which is an important factor in power absorption. A complete physical explanation of such phenomena needs more theoretical and experimental works after considering other plasma parameters also.

Figure 6 shows different power absorption channels in ^{3}He(H) and ^{4}He(H) plasmas with concentration. Quantitative values of power absorption through different channels are enumerated in table 3. The wave absorption by the minority H ion is better in ^{3}He(H) plasma than in ^{4}He(H) plasma (top panel of figure 6), whereas power absorption by electron is reverse (second panel from top of figure 6). For minority concentration, $\eta \leq 1\%$, the fast wave has undergone weak cyclotron damping at minority resonance layer in both ^{3}He(H) and ^{4}He(H) plasmas; but more prominent in ^{3}He(H) plasma. As the minority concentration is increased, the damping has increased until the absorption reaches a maximum value at a critical concentration, η_c. The η_c value for ^{3}He(H) plasma lies between 7% and 10% whereas that for ^{4}He(H) plasma lies between 3% and 5%. For further increase of minority concentration beyond the critical value, the wave polarisation becomes less favourable for cyclotron damping in the vicinity of minority resonance layer [11]. In ^{3}He(H) plasma there is no second harmonic power absorption by ^{3}He ion, whereas in ^{4}He(H) plasma second harmonic power absorption by ^{4}He ion decreases initially with concentration between 0.5% and $\eta = 1\%$ and again increases up to $\eta = 5\%$ and beyond that it decreases (third panel from the top of figure 6). An initial decrease in IBW absorption in ^{3}He(H) plasma is

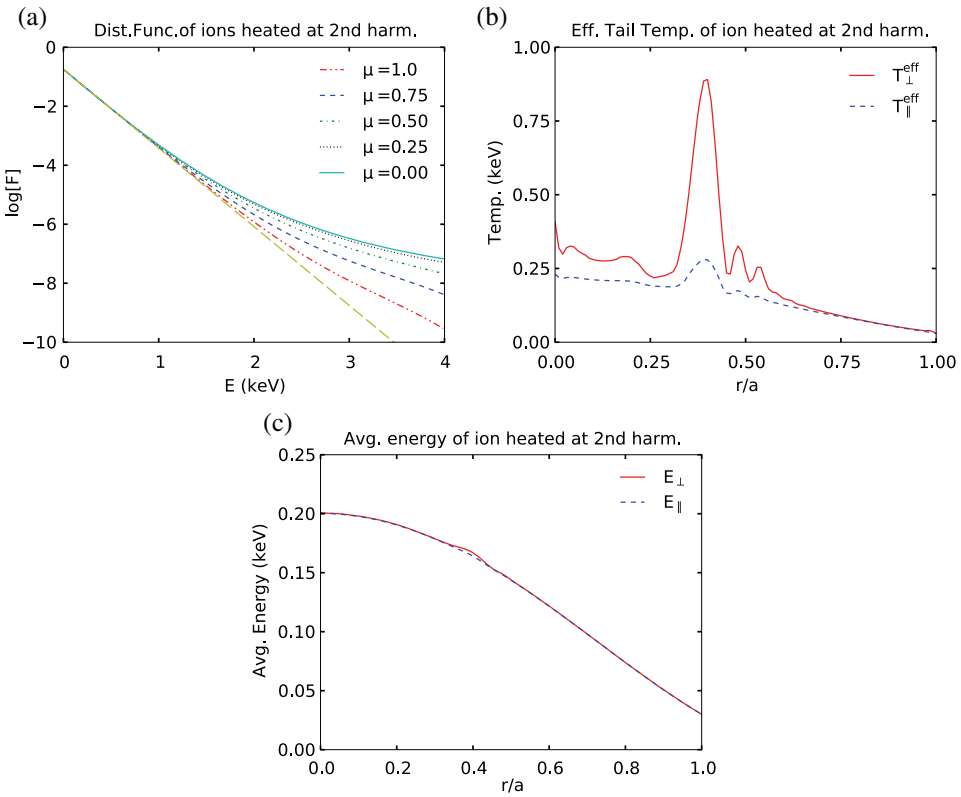

Figure 8. (**a**) Semi-log plots of quasilinear distribution function vs. energy at five values of the pitch angle (μ), at the position of peak absorption for the majority ion (^{4}He) heated at second harmonic. (**b**) shows the effective parallel and perpendicular tail temperature whereas (**c**) shows the effective average energy of the majority ion vs. normalised radius for a total coupled power of 0.1 MW. The long dashed curve is the unperturbed Maxwellian at peak absorption position and a background temperature of 0.200 keV.

also observed in the same concentration range 0.5% and 1% (bottom panel of figure 6). The decrease in absorption with concentration between 0.5% and 1% may be related to complex change in elements of dielectric tensor or some other complex phenomena related to wave polarisation. A rigorous theoretical calculation can only shed light on it. The IBW absorption by electron in ^{4}He(H) plasma is almost nil; but in the case of ^{3}He(H) plasma, except a drop in IBW absorption with concentration between 0.5% and 1% as has been mentioned earlier, it increases up to 3% of minority concentration and then decreases to a minimum at 7% minority concentration as shown in the bottom panel of figure 6.

In both ^{3}He(H) and ^{4}He(H) plasmas, minority heating and hence power absorption by minority ion is dominant throughout the minority concentration range. Beyond critical minority concentration, direct wave power absorption by electron starts to increase, whereas power absorption by electron from IBW produced from mode-conversion region decreases and even becomes zero in the case of ^{4}He(H) plasma (table 3) contradicting the general fact that with the increase of minority concentration, mode conversion and hence production of IBW increases. This apparent contradiction could be due to the fact that with the increase in minority concentration, ion–ion resonance layer and hence mode-conversion layer, very near to ion–ion resonance layer, gradually shifts towards in-board side of high field region of the tokamak. Due to gradual increase in length of the region between ion resonance layer and mode-conversion layer with increase in minority concentration, very less transmitted wave power from the resonance layer reaches the mode-conversion layer after direct wave power absorption by electrons in this region.

Now it is appropriate to present a few results from SSFPQL solver to show the effect of minority heating on distribution functions, and effective parallel and perpendicular temperatures of the energetic particles in the tail region of the distribution functions. More results and discussion from SSFPQL solver will be reported separately. The total coupled power is assumed to be 0.1 MW. In this report, only the results of ^{4}He(H) plasma will be shown because the results of minority heating of ^{3}He(H) plasma are almost the same as that of ^{4}He(H) plasma and there is no majority ion heating in ^{3}He(H) plasma as second harmonic resonance layer falls

outside the plasma for the chosen plasma parameters (see table 2).

Figure 7 shows semi-logarithmic plots of the quasi-linear distribution functions vs. energy for a few values of velocity pitch angle μ ($\mu = v_\parallel/v$ where $v_\parallel$, v are parallel and total velocities of the ion respectively) at the radial position corresponding to the maximum power absorption of minority ions (H ion) in ^{4}He(H) plasma of 5% minority concentration. The tails of the distribution functions of the minority ions are more energetic and hence more anisotropic (measured by the ratio of perpendicular and parallel components of the ion velocities) also. The effective perpendicular and parallel temperature (calculated from logarithmic energy derivatives) of the minority ions vs. normalised radius are shown in figure 7b. The effective perpendicular temperature (logarithmic energy derivative at $v_\parallel = 0$) of the tail of the minority ion ($\approx$25 keV) is much larger compared to the effective parallel temperature ($\approx$3 keV). Because of the modest effective temperature of the high-energy (suprathermal) tail, the average perpendicular and parallel energy of the minority ions are good as shown in figure 7c.

The same results are shown in figure 8 for the majority ions (^{4}He ion). Figure 8a is the distribution function of ^{4}He ion in semi-logarithm scale for the same μ values as taken in figure 7a. The tails of the distribution functions are less energetic and hence less anisotropic compared to those for minority ion. The power absorbed by helium ion is roughly an order of magnitude less than that by hydrogen ion. Therefore, not only the effective tail temperatures (8b) are much lower, but also the average parallel and perpendicular energies (8c) are less compared to those of the minority ions, hydrogen. It is expected because the contribution of high-energy (suprathermal) helium ions to the total energy is small. These phenomena are also in accordance with the well-known fact that the wave absorption by ions at second harmonic resonance relies on FLR effect and hence efficiency of this heating scheme depends critically on ion temperature [2,8] which, in our case is only 200 eV.

4. Summary

We have studied numerically the ICRH scenarios in two-species, low ion temperature plasma consisting of helium as majority and hydrogen as minority ions, to explain fundamental physics associated with minority heating and to assess its feasibility to attain H-mode with the help of ICRH code TORIC coupled with SSFPQL module taking SST-1 phase-I plasma parameters. In ^{3}He(H) and ^{4}He(H) plasmas, minority resonance layers are not shielded by ion–ion resonance and cut-off layers. Ion–ion resonance and cut-off layers lie on the high field side and move gradually towards in-board high field side with the increase of minority concentration. Hence ion–ion cut-off layer does not pose any obstacle to the wave to penetrate inside the plasma from the low field side to heat the minority ions at resonance layer. Coupling of the wave at the plasma–vacuum boundary in ^{4}He(H) plasma is better than that in ^{3}He(H) plasma. In both plasmas, ICRF wave energy mainly goes to ion due to minority heating in the chosen minority concentration range. Numerical analysis with the help of SSFPQL module shows that the tail of the distribution function of the minority ion is more energetic than that of the majority ion and, therefore, possesses modest effective temperature. Good coupling of wave in ^{4}He(H) and ^{3}He(H) plasmas as well as contribution of energetic minority ions from the tail region of the distribution function to the total energy make them ideal to study the ICRH scenarios in-depth to achieve enhanced mode in two-species low-temperature plasma.

Acknowledgements

The author wishes to thank Dr M Brambilla and Dr R Billato, Max Planck Institute for Plasma Physics (IPP), Garching, Germany for their help to make him understand the TORIC code and for giving him permission to use it.

References

[1] Y C Saxena, SST-1 Team, *Nucl. Fusion* **40**, 1069 (2000)
[2] M Brambilla, *Plasma Phys. Control. Fusion* **41**, 1 (1999)
[3] M Brambilla and R Bilato, *Nucl. Fusion* **46**, S387 (2006)
[4] M Brambilla, *Kinetic theory of plasma waves – Homogeneous plasma* (Oxford University Press, New York, 1998)
[5] T H Stix, *Waves in plasma* (American Institute of Physics, New York, 1992)
[6] L-G Eriksson, M J Mantsinen, F G Rimini, F Nguyen, C Gormezano, D F H Start and A Gondhalekar, *Nucl. Fusion* **38**, 265 (1998)
[7] F W Perkins, *IEEE Trans. Plasma Sci.* **PS-12**, 53 (1984)
[8] M Brambilla, *Plasma Phys. Control. Fusion* **31**, 723 (1989)
[9] M Brambilla, *Nucl. Fusion* **34**, 1121 (1994)
[10] D J Griffiths, *Introduction to electrodynamics* (Prentice Hall of India Private Limited, New Delhi, 1984)
[11] J Wesson, *Tokamaks* (Oxford University Press, Oxford 2011)